Theoretical Characterization of the Air-Stable, High-Mobility Dinaphtho[2,3-*b*:2′3′-*f*]thieno[3,2-*b*]-thiophene Organic Semiconductor

Roel S. Sánchez-Carrera,*,† Sule Atahan,*,† Joshua Schrier,‡ and Alán Aspuru-Guzik*,†

Department of Chemistry and Chemical Biology, Harvard University, Cambridge, Massachusetts 02138, and Department of Chemistry, Haverford College, Haverford, Pennsylvania 19041

Received: October 22, 2009; Revised Manuscript Received: December 22, 2009

Recently, an optimum mobility of 8.3 $cm^2/(Vs)$ has been measured for single-crystal organic field-effect transistors based on the dinaphtho[2,3-*b*:2′,3′-*f*]thieno[3,2-*b*]-thiophene (DNTT) molecule. Here, on the basis of quantum chemistry calculations and molecular dynamics simulations, we investigate the microscopic charge transport parameters of the DNTT molecule and crystal. Our findings confirm that the moderate anisotropy of the hole mobility in DNTT is highly dependent on the presence of in-plane herringbonelike intermolecular interactions with large electronic coupling (transfer integral) values (ca. 0.1 eV). Also, we demonstrate that the π-extended heteroaromatic structure leads to strong electronic coupling interactions among neighboring molecules and to a decrease of the intramolecular reorganization energy. In DNTT, thermal modulations of the electronic couplings at 300 K remain small when compared to those exhibited by the pentacene single crystal. This theoretical study suggests that heteroacenes are a promising route toward high-mobility organic semiconductor materials. Charge transport is discussed in the framework of both band and hopping models.

I. Introduction

Organic semiconductors are widely investigated as candidates for new generation of thinner, larger, and higher resolution electronic devices.[1–4] Advances in the scientific understanding and in the device performance of these materials have resulted in organic semiconducting materials that have, in some instances, superseded Si in performance.[5–8] Among them, the pentacene molecular crystal, which has emerged as the benchmark of organic molecular semiconductors, has been used to develop organic thin-film transistors with hole mobilities as high as 5.5 $cm^2/(Vs)$.[9] However, building materials with both air stability and high charge mobility has proved to be a very challenging task.[1,10–12]

Recently, a new molecular semiconductor, dinaphtho[2,3-*b*:2′,3′-*f*]thieno[3,2-*b*]-thiophene (DNTT) was introduced by Takimiya and co-workers[13] and has gained attention due to its high air-stable mobility values (3.1 $cm^2/(Vs)$)[14] and its relatively simple synthetic pathway. In addition, a more recent study reported an optimum mobility of ~8.3 $cm^2/(Vs)$ in the saturation regime of single-crystal organic field-effect transistors based on DNTT.[15] Recent experimental measurements also revealed a moderate anisotropy of the charge mobility of DNTT single-crystal transistors.[16] Despite the availability of the experimental evidence of the high-performance of the DNTT molecular crystal, to the best of our knowledge, there is no theoretical characterization that provides a clear explanation for the origin of its high mobility and moderate anisotropic behavior.

Here, we use quantum-chemical calculations and molecular dynamics simulations to investigate the charge transport characteristics of DNTT in terms of the electronic and vibrational couplings of both the molecule and the crystal. The crystalline structure of DNTT is characterized by the presence of herringbone sheets (*ab* plane) with relatively weak coupling between the layers (*c* axis). We find that the herringbone packing of DNTT molecules plays a significant role in determining the observed moderate anisotropy of the hole mobilities in DNTT. This, in part, is due to the presence of strong electronic couplings between molecular dimers located in the direction of the *ab* plane. We also find that the microscopic charge transport properties in DNTT are only slightly perturbed by the electron−phonon interactions, unlike in small oligoacene organic semiconductors (i.e., naphthalene and anthracene) or in oligothiophene-based semiconducting materials, where the vibrational couplings play an important role in the description of the transport properties of these materials.[17–20] Comparison with experiment and pentacene, the well-known organic semiconductor material, is also highlighted.

II. Computational Methodology

The geometry and electronic structure of the isolated DNTT molecule were obtained at the density functional theory (DFT) level by performing geometry optimizations with the Becke-three parameter Lee−Yang−Parr (B3LYP) hybrid density functional[21,22] and the 6-31G(d,p) basis set,[23–25] as implemented in the Q-Chem software package.[26] The results of vibrational frequency calculations at the B3LYP/6-31G(d,p) level of theory were then used to calculate the relaxation energy based on the theoretical methodology described by Reimers[27] and adapted here for the Q-Chem code. The transfer integrals for nearest-neighbor pairs of DNTT molecules were also calculated at the same level of theory.

The electronic-band structure calculation of the DNTT single-crystal was carried out using DFT with the PBE[28] (Perdew−Burke−Ernzerhof) exchange-correlation functional and plane-wave basis set as implemented in the VASP code.[29–31] Electron-ion interactions were described using the projector augmented wave (PAW) method.[32,33] The kinetic energy cutoff on the wave function expansion was 300 eV, and the self-

* To whom correspondence should be addressed. E-mail: rsanchez@fas.harvard.edu (R.S.S.-C.); atahan@fas.harvard.edu (S.A.); aspuru@chemistry.harvard.edu (A.A.-G.).
† Harvard University.
‡ Haverford College.

10.1021/jp910102f
Published on Web 01/19/2010

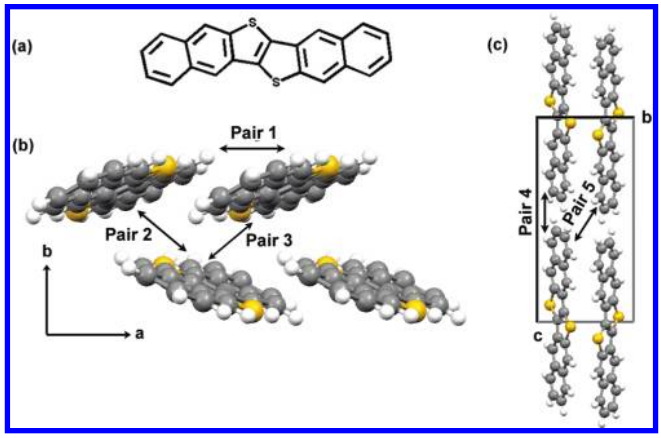

Figure 1. (a) Chemical structure of DNTT. (b) Crystal structure of DNTT in the *ab* plane. (c) Crystal structure of DNTT in the *bc* plane ($a = 6.187$, $b = 7.662$, $c = 16.21$ Å; $\beta = 92.49$).[13] Labels correspond to the DNTT molecular pairs used in the calculation of transfer integrals.

consistent calculations were carried out with a 14 × 14 × 12 *k*-point mesh. The inverse effective mass tensor was calculated using Sperling's centered difference method at the valence band edge of DNTT with $dk = 0.02$ (2π/Å).

To investigate the modulation of the transfer integrals by the thermal motions in the crystal (see electron-vibration coupling section below), we employed a combined approach that uses molecular dynamics (MD) simulations and quantum-chemical calculations. First, a 4 × 4 × 4 supercell containing 128 molecules was created using replicas of the experimentally determined DNTT unit cell. To describe the interatomic potentials in the DNTT crystal, we used the MM3 force field with the addition of electrostatic potential charges obtained at the B3LYP/6-31G(d,p) level of theory. All bonds to hydrogen atoms were constrained at ideal bond lengths with the help of RATTLE algorithm.[34] A 250 ps simulation was performed with time steps of 2 fs in NVT ensemble for $T = 300$ K with periodic boundary conditions. Only the last 150 ps of the total simulation time were included in our analysis. The atomic coordinates of the supercell were saved every 30 fs along the trajectory to give 5000 total snapshots. All nuclear dynamics in this work were carried out with TINKER 4.2 molecular modeling package.[35–37] Finally, the atomic coordinates of the three different molecular dimers, illustrated in Figure 1b, were extracted from the MD snapshots and used to calculate transfer integrals at the B3LYP/6-31G(d,p) level of theory. The results of the 15000 ab initio evaluations of the intermolecular electronic couplings were used to estimate the strength of the nonlocal source of electron−phonon interactions.

The reported crystalline structure of DNTT based on the X-ray structural analysis has almost planar molecules packed along the *ab* plane in the typical herringbone structure.[13] The monoclinic unit cell, which belongs to the $P2_1$ space group, involves two translationally nonequivalent molecules, giving rise to different types of dimer interactions, as illustrated in Figure 1. In this work, we use the previously reported crystalline structure of DNTT and the generalized methodology described above to investigate the electronic properties and the vibrational couplings of this high-performance organic molecular semiconductor.

III. Results and Discussion

We investigated the microscopic charge transfer characteristics of DNTT in terms of its transfer integrals, electronic band structure, effective masses, and local and nonlocal electron−phonon interactions. Below, we discuss our main findings relevant to the description of the charge transport properties in the DNTT crystal.

TABLE 1: DFT Estimates of the Transfer Integral for Molecular Pairs in the DNTT Crystal (See Figure 1 for Labeling)

	hole (meV)	electron (meV)	hole (meV)[a]
t_a, pair 1	81	−27	79
t_{d_1}, pair 2	28	37	52
t_{d_2}, pair 3	−94	−45	86
t_{c_1}, pair 4	13	0	−
t_{c_2}, pair 5	0	8	−

[a] Calculation based on extended Hückel molecular orbitals from ref 16 for comparison.

A. Transfer Integrals and Electronic Band Structure. The electronic properties of single crystals of organic molecules are generally associated with the study of intermolecular transfer integrals (t) and their respective bandwidths (W). Within a simple tight-binding model the valence [conduction] bandwidth results from the interactions of the highest-occupied molecular orbital (HOMO) [lowest-unoccupied molecular orbital (LUMO)] levels of each independent molecule within the crystal.[38] For instance, in the case of an infinite one-dimensional crystalline stack of molecules the total bandwidth W is equal to $4t$.[39,40] In a simpler model, involving only two interacting molecules, the splitting of the HOMO [LUMO] energy levels on the two molecules is equal to $2t$.[38] However, when the two interacting molecules are not symmetrically equivalent, the energy-splitting model leads to inaccurate results due to site energy differences induced by electrostatic effects such as polarization.[41] Here, we employ a more rigorous computational method, similar to those developed by Norton et al.[42] and Senthilkumar et al.,[43] to estimate transfer integrals between the molecular dimers shown in Figure 1.

The calculated transfer integrals of the selected molecular dimers in the *ab* plane and along the *c* axis of the DNTT molecular crystal are given in Table 1. Note that the sign of the transfer integrals for holes and electrons changes among the different molecular pairs in DNTT and depends on the symmetry of the molecular wave function and the crystal structure of the investigated molecular system (for additional details see Supporting Information and ref 44). Despite differences in the sign convention of the transfer integrals, our results are in good agreement with recent calculations reported by Uno et al.[16] In DNTT relatively large values of the transfer integral are found for dimers along the *a* axis (t_a, pair 1 in Figure 1b) and along the diagonal directions in the *ab* plane (t_{d_1} and t_{d_2}, pair 2 and pair 3 in Figure 1b, respectively). Interestingly, even though short intermolecular distances are found along the *c* axis (ranging between 2.5 and 3.5 Å), only small transfer integral values for holes and electrons are found along this direction. In this view, our calculated electronic couplings support the experimentally observed two-dimensional character of the charge transport properties in DNTT.[16] For comparison, the pentacene crystal shows a hole transfer integral value of 85 meV along the diagonal direction comparable to that of DNTT (−94 meV); however, along the π-stacking direction, the pentacene crystal presents a rather moderate hole transfer integral value of 36 meV, whereas the DNTT crystal shows a value that is twice as large along the same π-stacking direction (i.e., along the *a*-axis).

To gain a better understanding of the strength of the electronic couplings in the *ab* plane (i.e., the herringbone plane), we have also looked at the details of the three-dimensional electronic

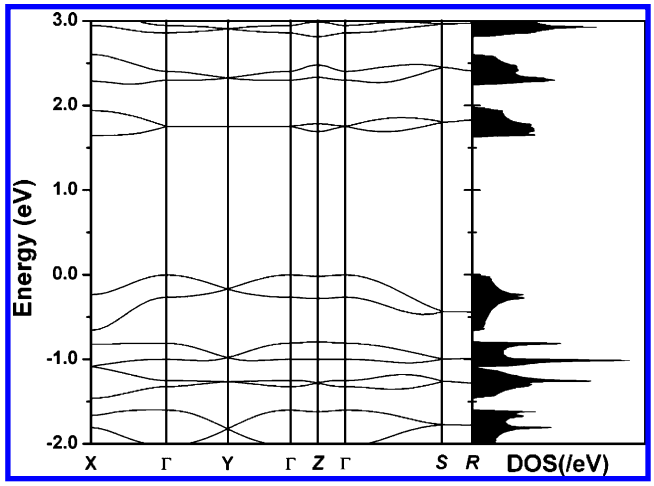

Figure 2. Calculated electronic band structure of the DNTT crystal. The valence band edge is located at the Γ-point. The right panel illustrates the corresponding density of states. The zero of energy levels corresponds to the valence band edge. The high-symmetry points in units of ($2\pi/a$, $2\pi/b$, $2\pi/c$) are Γ = (0,0,0), X = (0.5,0,0), Y = (0,0.5,0), Z = (0,0,0.5), S = (0.5,0.5,0), and R = (0.5,0.5,0.5).

band structure in DNTT. The calculated band structure along various high symmetry directions in reciprocal space is shown in Figure 2. Both the valence and conduction bands consist of two subbands arising primarily from the interaction of the HOMO and LUMO levels of the two translationally nonequivalent molecules present in the unit cell. Figure 2 also displays the calculated density of states (DOS), which shows that there are no contributions from other molecular states to either the valence or the conduction band. The estimated HOMO and LUMO bandwidths are about 670 and 370 meV, respectively. In this case, the HOMO bandwidth is slightly larger than that of the pentacene crystal (600 meV);[45] however, the LUMO bandwidth for the DNTT crystal is almost half of that previously reported for the pentacene crystal.[45]

The observed splitting into two subbands for the valence and conduction band highlights the presence of significant intermolecular interactions not only along the short crystalline axes but also along the diagonal directions within the herringbone plane. In fact, the largest valence band dispersion occurs along Γ-X and Γ-S, corresponding to the a^* and $a^* + b^*$ crystallographic directions, respectively. These results are consistent with the calculated transfer integrals (see Table 1), where significant electronic couplings are found for the π-stacked dimers (pair 1) and between the diagonal dimers (pairs 2 and 3). The Γ-Z direction corresponds to the c axis and is in agreement with the relatively small values of the transfer integrals for holes and electrons (t_{c_1} for holes and t_{c_2} for electrons ∼10 meV); only small amounts of valence- and conduction-band dispersion occur along this direction. The conduction band shares most of the relevant features of the valence band, with relative dispersion along the Γ-X, Γ-S, and Γ-Z directions. However, the main difference between the two transport-related bands occurs along the Γ-Y direction (b axis), along which the valence band has dispersion and the conduction band is completely flat. This difference can be understood by examination of the charge density patterns of the HOMO and LUMO wave functions (see Figure 4). For example, along the b axis, the electronic interactions occur mainly between the two translationally nonequivalent molecules in the crystal. Since the LUMO wave function lacks of significant electron density on the sulfur atoms, the effective overlap of the wave functions (and consequently the band dispersion) would be, in principle, smaller than that of the HOMO. On the other hand, the electron density present on the sulfur atoms of the HOMO level promotes effective electronic interactions and significant band dispersion, as observed in Figure 2.

TABLE 2: Hole Effective Mass m (in Units of the Free Electron Mass at Rest, m_0) Calculated at the Valence Band Edge of the DNTT Crystal

DNTT	m/m_0	parallel to
holes at Γ	1.89	$a + 0.050c$
	2.73	b
	5.28	$c - 0.046a$

In light of the recent mobility measurements of hole charge carriers in DNTT,[15,16] we apply the concept of effective mass to describe the charge transport characteristics in this high-performance organic semiconductor. In the case of wide bands, where the thermally populated levels remain close to the valence and conduction band edges, the mobility is governed by the electron effective masses that can be computed from the band structure at those band extrema. The tensor for the inverse effective mass (m_{ij}) is given by[46]

$$m_{ij}^{-1} = \frac{1}{\hbar^2}\frac{\partial^2 \varepsilon}{\partial k_i \partial k_j} \quad (1)$$

where subscripts i and j denote the Cartesian coordinates in reciprocal space, ε the band energy, $\hbar$ the Planck constant, and k the momentum. We have calculated the effective masses at the top of the valence band edge located at the Γ point in the DNTT crystal. The effective masses are then analytically derived by fitting eq 1 to a second-order polynomial; the calculated values are shown in Table 2.

The lightest hole in DNTT ($1.9m_0$) is found along the a axis, and a relatively small effective mass is found along the b-axis ($2.7m_0$). These results are, again, in good agreement with the calculated values of the transfer integrals (see Table 1). For comparison, the average of the hole effective masses for the different polymorphs of the pentacene crystal falls in the range of $1.0m_0$−$4.0m_0$.[45,47–49] Within this effective-mass approach, the anisotropy of m implies an anisotropic hole mobility μ with the highest mobility along the a axis and lower mobility along the b axis, as observed in the experiments[16] (one should note that according to the band regime[50] the carrier mobility μ and the effective mass m of the charge carrier are inversely proportional). By use of eq 3 (vide infra) and the effective masses reported in Table 2 the theoretical mobility ratio of μ_a/μ_b is approximately 1.44. This is within 10% of the experimentally measured mobility ratio, for which $\mu_a/\mu_b = 1.6$. Finally, in Figure 3, we plotted the calculated hole effective masses for all directions within the ab plane. Our calculations indicate only a moderate anisotropy of the hole effective masses in DNTT, in contrast to the very large anisotropy of the hole effective masses within the ab plane of pentacene.[45]

B. Electron-Vibration Coupling. In organic molecular crystals, there are two major sources of electron−phonon (vibration) interactions: local and nonlocal couplings.[51,52] The local electron−phonon coupling arises from the modulation of the site energies by intra- and intermolecular vibrations; its strength is commonly expressed, in the context of electron transfer theory, by the reorganization energy λ_{reorg}. Here, we discuss only the intramolecular geometry relaxation contributions to the local coupling, as the polarization of the surrounding molecules (i.e., intermolecular geometry relaxation contribu-

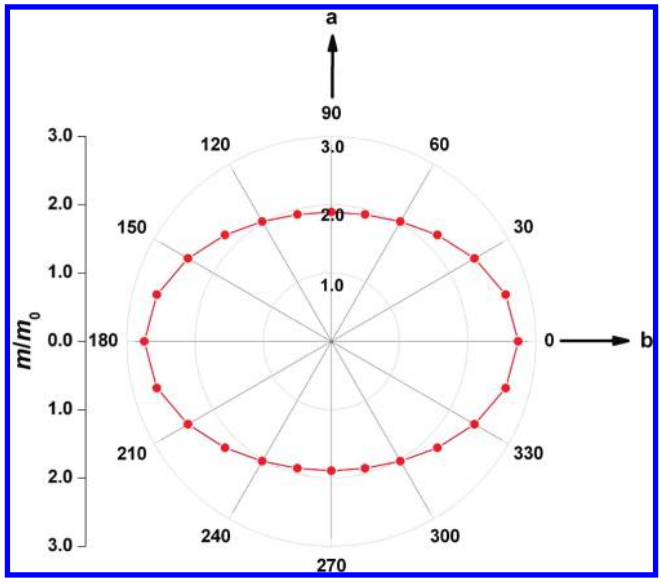

Figure 3. Hole effective masses m (in units of the electron mass at rest, m_0) calculated at the valence band edge of the DNTT crystal as function of the crystallographic direction.

tions) is expected to be significantly smaller.[53] In DNTT the intramolecular reorganization energies associated with the hole- and electron-vibrational couplings as calculated from adiabatic potentials are 130 and 202 meV, for holes and electrons, respectively. In comparison, the corresponding intramolecular λ_{reorg} in pentacene is approximately 97 and 132 meV, respectively.[54,55]

In Figure 4, we illustrate the contribution of each normal mode to the relaxation energy λ_{rel} (where $\lambda_{rel} \approx \lambda_{reorg}/2$) related to the formation of the radical−cation and radical−anion states (only the most strongly coupled modes are shown). The main difference in the λ_{rel} between holes and electrons in DNTT results from a significant drop in the vibronic coupling interaction with a high-frequency mode at around 1600 cm^{-1}; the magnitude of the coupling with all other modes remains more or less similar in both charged states. The marked decrease in the vibronic coupling interactions in DNTT can be understood in terms of the orbital vibronic coupling constants.[56,57] According to this model, the vibration coupling constants are large when the molecular deformation along the corresponding normal coordinate considerably distorts the electron density of the related molecular orbitals. In this case, the 1600 cm^{-1} high-energy mode consists of C−C stretching within the inner molecular rings. Because part of the electron density in the HOMO wave function of DNTT is located on the sulfur atoms, the energy of this molecular level is less affected by this vibration than that of the LUMO level, in which the electron density is mainly distributed across the six fused aromatic rings. Similar arguments describe the presence of a contributing normal mode to the hole-relaxation energy at around 450 cm^{-1}; this vibration involves stretches of the molecule along the short molecular axis via the sulfur atoms and shows no contribution to the electron-relaxation energy. Therefore, the presence/absence of electronic density on the sulfur atoms in the HOMO/LUMO wave function of these molecular orbitals provides an explanation for the relevance of this vibration (i.e., 450 cm^{-1}), uniquely to the description of the hole-relaxation energy, as shown in Figure 4.

The decomposition of the intramolecular reorganization energy into individual contributions from the relevant vibrational modes permits definition of the contribution of the low- and

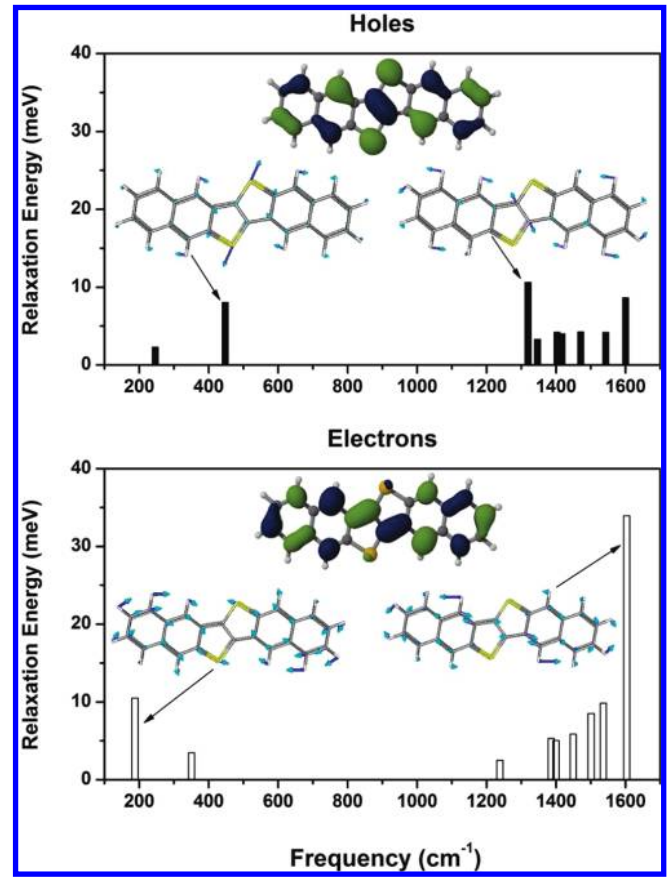

Figure 4. Contributions of the vibrational modes to the hole and electron relaxation energy in DNTT. The insets show the HOMO and LUMO wave functions and the normal modes with strong hole- and electron-vibronic coupling in DNTT.

high-frequency vibrations to the overall value of λ_{reorg}. Here, we looked at contributions of the low-frequency modes (below 500 cm^{-1}) related to hole transfer. We found that, in DNTT, 17% of the reorganization energy originates from low-frequency vibrations. In pentacene, these contributions account only for 2%,[55] and in pentathienoacene, the thiophene equivalent of pentacene, the contribution of the low-frequency vibrations (induced by the sulfur atoms) accounts for as much as 44% of the calculated intramolecular reorganization energy.[58] This result points toward the overall superior performance of hybrid thiophene−acene semiconductors, such as DNTT, in which the limited number of sulfur atoms (2 per molecular unit) reduces the contributions of the low-frequency vibrations to the reorganization energy without compromising the environmental stability of the molecule itself (previously, it has been demonstrated that functionalization of the molecular backbone with sulfur leads to compounds with an improved environmental stability and modified crystal packing).[59,60]

The second source of electron−phonon interactions, namely, the nonlocal coupling, arises from the modulation of the transfer integrals (mainly) by intermolecular vibrations.[52] Unlike inorganic semiconductors, in an organic semiconductor the molecules are held together by weak forces, therefore the transfer integrals in organic materials are very susceptible to the thermal fluctuations of the molecules within the crystal. To a good approximation, the overall strength of the nonlocal interactions can be obtained by considering the variance of the transfer integrals due to thermal fluctuations.[17,61,62] To analyze the effect of nonlocal electron−phonon coupling on transfer integrals, we use a methodology that combines MD simulations and ab initio

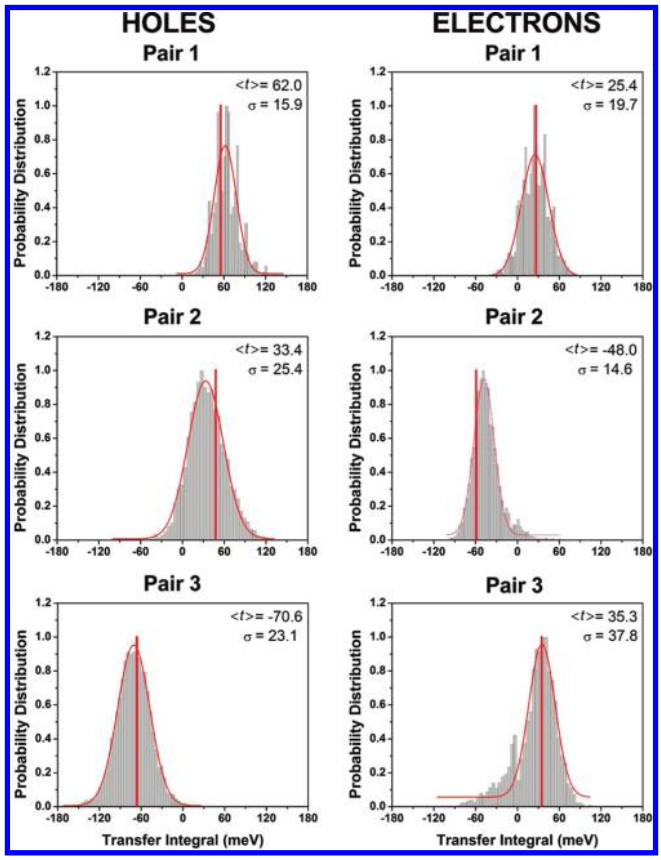

Figure 5. Normalized probability distribution of the transfer integrals for holes and electrons in pair 1, pair 2, and pair 3 of the DNTT crystal. The average value $\langle t \rangle$ and the standard deviation σ are also reported. The single vertical lines correspond to transfer integrals calculated at the equilibrium configuration of the MD simulation.

quantum-chemistry methods. While MD simulations permits access to all (inter- and intramolecular) vibrational modes in the crystal, ab initio quantum-chemical calculations are used to estimate values of the transfer integrals for selected molecular dimers; whose coordinates are extracted from the MD trajectory at regular time intervals. This combined approach represents an extension of the work of Troisi and co-workers,[62,63] and when applied to organic solids relevant to the field of organic electronics,[62,64–66] it yields a quasi-Gaussian distribution of the transfer integrals as sampled by classical MD simulations (see Figure 5).

In Figure 5, the distributions of the transfer integrals for holes and electrons for pair 1, 2, and 3 of the DNTT crystal are presented. The standard deviations σ of the transfer integrals are also indicated in Figure 5. According to Coropceanu et al.,[17] the standard deviation of the transfer integrals, as derived from MD simulations, can be used to estimate the overall strength of the nonlocal contribution (L)

$$L = \sigma^2/(2k_B T) \tag{2}$$

where k_B is the Boltzmann constant and T the temperature. L has a physical meaning similar to that of the reorganization energy in the case of the local electron−phonon coupling mechanism.[17] This parameter quantifies the total strength of the nonlocal electron−phonon coupling mechanism and, in the high-temperature limit, defines the degree of variance of the transfer integrals due to phonon vibrations. By use of eq 2, we estimate the values of L at room temperature for both holes and electrons in the three representative dimers in the *ab* plane of the DNTT crystal. We find that for most of the selected molecular dimers L falls in the range of 5−15 meV for both holes and electrons. These values of L are 5 or more times smaller than the calculated transfer integrals obtained at the equilibrium configuration of the MD simulation (see Supporting Information). Thus, the contribution of the nonlocal interactions appears to be too weak to result in any significant vibration-modulated contribution to the charge transport properties in DNTT.

As a comparison, the estimated value of L for holes in DNTT along the diagonal direction (along the so-called herringbone direction) are even smaller than those obtained along a similar orientation in the pentacene crystal (for example, in the case of pentacene, $L = 21$ meV for herringbone dimers).[65] In a similar spirit, although a different Hamiltonian was employed to compute the transfer integrals, the recent theoretical investigations of Sleigh et al.[67] also support the above arguments. For instance, in ref 67, the estimated standard deviations of the hole transfer integrals in the pentacene crystal are almost twice as large as the ones calculated for the DNTT crystal.

C. Band and Hopping Transport Mechanisms. Despite the extensive use of the Holstein−Peierls molecular model[20,61,68–70] to derive qualitative interpretations of the experimental measurements of the charge-carrier mobilities in organic materials, the complete description of the charge-transport mechanism in organic semiconducting materials still represents a major challenge.[51,52]

This is further complicated by the sensitivity of experimental charge carrier mobility measurements to disorder, impurities, temperature, electric field, and carrier density.[52] Understanding the current limitations of the transport theories in molecular crystals and the fact that only hole mobilities have been reported for DNTT, in this study, we took the above-discussed parameters (i.e., effective masses, intramolecular reorganization energies, and the various transfer integrals) to estimate the hole mobilities in DNTT in limiting transport regimes, namely, the band and hopping regimes.

According to band-transport theory, the charge moves coherently in a wavelike manner and is scattered by phonons as the temperature increases. The carrier mobility in wide band materials is given by[46]

$$\mu = \frac{q\tau}{m} \tag{3}$$

where q is the charge, τ the mean free time between collisions (or the mean relaxation time of the band state), and m the effective mass of the charge carrier. In the isotropic relaxation time approximation, the mobility and its orientational anisotropy are dictated by the carrier effective mass (see Table 2).

By use of eq 3 and the effective masses from Table 2, we expect hole transport in DNTT to occur predominantly in the *ab* plane. As discussed in section IIIA, the calculated ratio for the mobilities along the *a* and *b* crystallographic axes is approximately 1.44. This makes charge transport less dependent on the molecular orientation, simplifying the construction of high-performance field-effect transistor designs. In contrast, the previously calculated hole-effective masses of pentancene[45] indicate an effective mobility ratio in the direction of the *ab* crystallographic plane that is an order of magnitude larger than that found in DNTT. Consequently, this leads to variability in organic field-effect transistor performance depending on the orientation of the molecular crystal with respect to the electrodes.

When the electron−phonon interactions are of the same order of magnitude as the electronic coupling (or transfer integral), the motion of the charge carriers can be modeled as a sequence of uncorrelated hops.[71,72] In the high-temperature limit, the charge carrier transfer rate k (or hopping rate) and, hence, the mobility can be approximated by the semiclassical form of Marcus theory given by[38]

$$k = \frac{t^2}{\hbar}\sqrt{\frac{\pi}{\lambda k_B T}}\exp\left[-\frac{\lambda}{4k_B T}\right] \quad (4)$$

Here, we approximated λ to be equal to λ_{reorg} (vide supra), and t represents the electronic coupling or transfer integral. The charge carrier transfer rates, k_i, between each of the various molecular dimers shown in Figure 1, are then used to calculate the hole diffusion coefficient (D)

$$D = \frac{1}{2n}\sum_i r_i^2 k_i P_i \quad (5)$$

where $n = 3$ is the dimensionality, k_i is the charge carrier hopping rate to the ith molecular neighbor, r_i is the distance to neighbor i, and P_i is the relative probability for charge transfer to a particular ith neighbor

$$P_i = k_i / \sum_i k_i \quad (6)$$

From the Einstein relation, the hole mobility is given as:

$$\mu = \frac{q}{k_B T} D \quad (7)$$

By use of eq 7, the hole transfer integrals reported in Table 1, the intramolecular hole reorganization energy, and $T = 300$ K, we estimated the hole mobility in DNTT to be approximately equal to 1.8 $cm^2/(Vs)$, in good agreement with experimentally observed mobilities of DNTT polycrystalline thin-film transistors.[13] By use of a similar procedure, we calculated the hole mobility in pentacene to be equal to 2.1 $cm^2/(Vs)$. At first sight, this result suggests a larger theoretically estimated hole mobility for the pentacene molecular crystal than that of DNTT. However, it is important to note that eq 7 does not account for the inclusion of the modulation of the transfer integrals by thermally activated vibrations (i.e., the nonlocal coupling effect), which we have estimated to be larger in pentance than in DNTT. Therefore, a more comprehensive comparison between these two molecular crystals, in the high-temperature limit, might result with the development of models that allow for the inclusion of the nonlocal vibrational couplings with both low- and high-frequency phonons, as demonstrated in several recent works.[17,73,74]

IV. Conclusions

We have investigated the electronic and vibrational couplings in the molecular and crystalline forms of the DNTT molecule. The transfer integral and band structure calculations confirm that the transport of the positive charge carriers is mostly two-dimensional along the *ab* plane, where herringbonelike intermolecular interactions are dominant. Only slight dispersion and relatively small values of the transfer integrals are found along the *c* axis, which is almost perpendicular to the herringbone plane. Consistent with recent experimental measurements, calculated effective masses in the *ab* plane explain the moderate anisotropy observed in the hole mobility of the DNTT crystal, in contrast to the large anisotropy of the hole effective masses previously reported for the pentacene crystal.

Our results also indicate that the sulfur atoms in DNTT play a dual role in the description of its microscopic charge transport properties: (1) they promote significant overlap of the molecular orbitals via intermolecular S···S interactions, and (2) although the members of the oligothiophene family of organic semiconductors are characterized by large intramolecular reorganization energies due to low-frequency vibrations induced by the sulfur atoms, the *limited* presence of sulfur atoms in DNTT (two atoms per molecular unit) accounts for the reduction in the value of the intramolecular reorganization energy. Overall, the results of the present work suggest that the hybridization of different molecular fragments (thiophene and acene) represents a viable route for the design of new organic semiconductors with superior charge transport properties. Thus, a combinatorial approach for finding novel heteroacene molecular structures is a very promising research direction.

The role of the nonlocal electron−phonon couplings in DNTT has been also investigated. Not surprisingly, the π-extended heteroaromatic molecular structure of DNTT, with its six fused aromatic rings (that is, a relative high molecular-weight-compound) and strong intermolecular electronic couplings, leads to relatively weak nonlocal electron−phonon couplings at room temperature. However, more systematic studies, for example MD simulations at different temperatures, are required to effectively assess the role of the intermolecular vibrations in the DNTT molecular crystal.

Finally, to shed light on the investigation of the charge transport mechanisms in DNTT, we estimated the hole mobilities in the context of both the band and hopping models. Our predicted results suggest that in the band transport regime DNTT might have an overall superior performance than pentacene, the benchmark for organic semiconductor. However, the interplay between these limiting regimes is an open question awaiting experimental evidence into the role played by low- and high-frequency vibrations in transport properties of organic molecular crystals.

Acknowledgment. We thank J. Krich, D. Rappoport, A. Perdomo, and L. Vogt for stimulating discussions. R.S.S.-C. thanks the Mary-Fieser Postdoctoral Fellowship at Harvard University. This work was also supported through a National Science Foundation Grant via Harvard MRSEC, Grant No. DMR-08-20484. We thank the High Performance Technical Computing Center at the Faculty of Arts and Sciences of Harvard University for invaluable support.

Supporting Information Available: DFT estimates of the transfer integral for molecular pairs in the DNTT calculated at the equilibrium configuration of the MD simulation, HOMO dimer molecular orbitals for pair 1, 2, and 3 in DNTT, DFT estimates of the relaxation energy related to hole and electron transport of DNTT, and DFT/MD estimates of the contributions of the nonlocal hole- and electron−phonon interactions in DNTT. This material is available free of charge via the Internet at http://pubs.acs.org.

References and Notes

(1) Anthony, J. E. *Chem. Rev.* **2006**, *106*, 5028–5048.

(2) Bendikov, M.; Wudl, F.; Perepichka, D. F. *Chem. Rev.* **2004**, *104*, 4891–4945.
(3) Fichou, D.; Bachet, B.; Demanze, F.; Billy, I.; Horowitz, G.; Garnier, F. *Adv. Mater.* **1996**, *8*, 500–504.
(4) Garnier, F.; Horowitz, G.; Peng, X. H.; Fichou, D. *Adv. Mater.* **1990**, *2*, 592–594.
(5) Jurchescu, O. D.; Baas, J.; Palstra, T. T. M. *Appl. Phys. Lett.* **2004**, *84*, 3061–3063.
(6) Podzorov, V.; Menard, E.; Borissov, A.; Kiryukhin, V.; Rogers, J. A.; Gershenson, M. E. *Phys. Rev. Lett.* **2004**, *93*, 086602.
(7) Reese, C.; Chung, W. J.; Ling, M. M.; Roberts, M.; Bao, Z. N. *Appl. Phys. Lett.* **2006**, *89*, 202108.
(8) Sundar, V. C.; Zaumseil, J.; Podzorov, V.; Menard, E.; Willett, R. L.; Someya, T.; Gershenson, M. E.; Rogers, J. A. *Science* **2004**, *303*, 1644–1646.
(9) Lee, S.; Koo, B.; Shin, J.; Lee, E.; Park, H.; Kim, H. *Appl. Phys. Lett.* **2006**, *88*, 162109.
(10) Anthony, J. E. *Angew. Chem., Int. Ed.* **2008**, *47*, 452–483.
(11) Chen, M. C.; Kim, C.; Chen, S. Y.; Chiang, Y. J.; Chung, M. C.; Facchetti, A.; Marks, T. J. *J. Mater. Chem.* **2008**, *18*, 1029–1036.
(12) Tang, M. L.; Reichardt, A. D.; Miyaki, N.; Stoltenberg, R. M.; Bao, Z. *J. Am. Chem. Soc.* **2008**, *130*, 6064–6065.
(13) Yamamoto, T.; Takimiya, K. *J. Am. Chem. Soc.* **2007**, *129*, 2224–2225.
(14) Yamamoto, T.; Takimiya, K. *J. Photopolym. Sci. Technol.* **2007**, *20*, 57–59.
(15) Haas, S.; Takahashi, Y.; Takimiya, K.; Hasegawa, T. *Appl. Phys. Lett.* **2009**, 95.
(16) Uno, M.; Tominari, Y.; Yamagishi, M.; Doi, I.; Miyazaki, E.; Takimiya, K.; Takeya, J. *Appl. Phys. Lett.* **2009**, *94*, 223308.
(17) Coropceanu, V.; Sánchez-Carrera, R. S.; Paramonov, P.; Day, G. M.; Brédas, J. L. *J. Phys. Chem. C* **2009**, *113*, 4679–4686.
(18) da Silva Filho, D. A.; Coropceanu, V.; Fichou, D.; Gruhn, N. E.; Bill, T. G.; Gierschner, J.; Cornil, J.; Brédas, J. L. *Philos. Trans. R. Soc. a* **2007**, *365*, 1435–1452.
(19) Grozema, F. C.; van Duijnen, P. T.; Berlin, Y. A.; Ratner, M. A.; Siebbeles, L. D. A. *J. Phys. Chem. B* **2002**, *106*, 7791–7795.
(20) Hannewald, K.; Stojanovic, V. M.; Schellekens, J. M. T.; Bobbert, P. A.; Kresse, G.; Hafner, J. *Phys. Rev. B* **2004**, *69*, 075211.
(21) Becke, A. D. *J. Chem. Phys.* **1993**, *98*, 5648–5652.
(22) Lee, C. T.; Yang, W. T.; Parr, R. G. *Phys. Rev. B* **1988**, *37*, 785–789.
(23) Francl, M. M.; Pietro, W. J.; Hehre, W. J.; Binkley, J. S.; Gordon, M. S.; Defrees, D. J.; Pople, J. A. *J. Chem. Phys.* **1982**, *77*, 3654–3665.
(24) Hariharan, P. C.; Pople, J. A. *Theor. Chim. Acta* **1973**, *28*, 213–222.
(25) Hehre, W. J.; Ditchfie, R.; Pople, J. A. *J. Chem. Phys.* **1972**, *56*, 2257–2261.
(26) Shao, Y.; Molnar, L. F.; Jung, Y.; Kussmann, J.; Ochsenfeld, C.; Brown, S. T.; Gilbert, A. T.; Slipchenko, L. V.; Levchenko, S. V.; O'Neill, D. P.; DiStasio, R. A., Jr.; Lochan, R. C.; Wang, T.; Beran, G. J.; Besley, N. A.; Herbert, J. M.; Lin, C. Y.; Van Voorhis, T.; Chien, S. H.; Sodt, A.; Steele, R. P.; Rassolov, V. A.; Maslen, P. E.; Korambath, P. P.; Adamson, R. D.; Austin, B.; Baker, J.; Byrd, E. F.; Dachsel, H.; Doerksen, R. J.; Dreuw, A.; Dunietz, B. D.; Dutoi, A. D.; Furlani, T. R.; Gwaltney, S. R.; Heyden, A.; Hirata, S.; Hsu, C. P.; Kedziora, G.; Khalliulin, R. Z.; Klunzinger, P.; Lee, A. M.; Lee, M. S.; Liang, W.; Lotan, I.; Nair, N.; Peters, B.; Proynov, E. I.; Pieniazek, P. A.; Rhee, Y. M.; Ritchie, J.; Rosta, E.; Sherrill, C. D.; Simmonett, A. C.; Subotnik, J. E.; Woodcock, H. L., 3rd; Zhang, W.; Bell, A. T.; Chakraborty, A. K.; Chipman, D. M.; Keil, F. J.; Warshel, A.; Hehre, W. J.; Schaefer, H. F., 3rd; Kong, J.; Krylov, A. I.; Gill, P. M.; Head-Gordon, M. *Phys. Chem. Chem. Phys.* **2006**, *8*, 3172–91.
(27) Reimers, J. R. *J. Chem. Phys.* **2001**, *115*, 9103–9109.
(28) Perdew, J. P.; Burke, K.; Ernzerhof, M. *Phys. Rev. Lett.* **1996**, *77*, 3865–3868.
(29) Kresse, G.; Furthmuller, J. *Comput. Mater. Sci.* **1996**, *6*, 15–50.
(30) Kresse, G.; Hafner, J. *Phys. Rev. B* **1993**, *47*, 558.
(31) Kresse, G.; Hafner, J. *Phys. Rev. B* **1994**, *49*, 14251.
(32) Blochl, P. E. *Phys. Rev. B* **1994**, *50*, 17953–17979.
(33) Kresse, G.; Joubert, D. *Phys. Rev. B* **1999**, *59*, 1758–1775.
(34) Andersen, H. C. *J. Comput. Phys.* **1983**, *52*, 24–34.
(35) Dudek, M. J.; Ponder, J. W. *J. Comput. Chem.* **1995**, *16*, 791–816.
(36) Kundrot, C. E.; Ponder, J. W.; Richards, F. M. *J. Comput. Chem.* **1991**, *12*, 402–409.
(37) Ponder, J. W.; Richards, F. M. *J. Comput. Chem.* **1987**, *8*, 1016–1024.
(38) Pope, M.; Swenberg, C. E. *Electronic processes in organic crystals and polymers*, 2nd ed.; Oxford University Press: New York, 1999.
(39) Haddon, R. C.; Siegrist, T.; Fleming, R. M.; Bridenbaugh, P. M.; Laudise, R. A. *J. Mater. Chem.* **1995**, *5*, 1719–1724.
(40) Huang, J. S.; Kertesz, M. *J. Chem. Phys.* **2005**, *122*, 234707.
(41) Valeev, E. F.; Coropceanu, V.; da Silva Filho, D. A.; Salman, S.; Brédas, J. L. *J. Am. Chem. Soc.* **2006**, *128*, 9882–9886.
(42) Norton, J. E.; Brédas, J. L. *J. Chem. Phys.* **2008**, *128*, 034701.
(43) Senthilkumar, K.; Grozema, F. C.; Bickelhaupt, F. M.; Siebbeles, L. D. A. *J. Chem. Phys.* **2003**, *119*, 9809–9817.
(44) Berlinsk, A. J.; Carolan, J. F.; Weiler, L. *Solid State Commun.* **1974**, *15*, 795–801.
(45) de Wijs, G. A.; Mattheus, C. C.; de Groot, R. A.; Palstra, T. T. M. *Synth. Met.* **2003**, *139*, 109–114.
(46) Seeger, K. *Semiconductor physics: an introduction*, 9th ed.; Springer: Berlin; New York, 2004.
(47) Kitamura, M.; Arakawa, Y. *J. Phys.: Condens. Matter* **2008**, *20*, 184011.
(48) Troisi, A.; Orlandi, G. *J. Phys. Chem. B* **2005**, *109*, 1849–1856.
(49) Yoshida, H.; Sato, N. *Phys. Rev. B* **2008**, *77*, 235205.
(50) Sze, S. M. *Semiconductor devices, physics and technology*, 2nd ed.; Wiley: New York, 2002.
(51) Brédas, J. L.; Beljonne, D.; Coropceanu, V.; Cornil, J. *Chem. Rev.* **2004**, *104*, 4971–5003.
(52) Coropceanu, V.; Cornil, J.; da Silva Filho, D. A.; Olivier, Y.; Silbey, R.; Brédas, J. L. *Chem. Rev.* **2007**, *107*, 2165–2165.
(53) Norton, J. E.; Brédas, J. L. *J. Am. Chem. Soc.* **2008**, *130*, 12377–12384.
(54) Coropceanu, V.; Malagoli, M.; da Silva Filho, D. A.; Gruhn, N. E.; Bill, T. G.; Brédas, J. L. *Phys. Rev. Lett.* **2002**, *89*, 275503.
(55) Malagoli, M.; Coropceanu, V.; da Silva Filho, D. A.; Brédas, J. L. *J. Chem. Phys.* **2004**, *120*, 7490–7496.
(56) Bersuker, I. B. *The Jahn-Teller effect*; Cambridge University Press: Cambridge, United Kingdom, 2006.
(57) Kato, T.; Yamabe, T. *J. Chem. Phys.* **2005**, *123*, 024301.
(58) Kim, E.-G.; Coropceanu, V.; Gruhn, N. E.; Sánchez-Carrera, R. S.; Snoeberger, R.; Matzger, A. J.; Brédas, J.-L. *J. Am. Chem. Soc.* **2007**, *129*, 13072–13081.
(59) Laquindanum, J. G.; Katz, H. E.; Lovinger, A. J. *J. Am. Chem. Soc.* **1998**, *120*, 664–672.
(60) Wex, B.; Kaafarani, B. R.; Schroeder, R.; Majewski, L. A.; Burckel, P.; Grell, M.; Neckers, D. C. *J. Mater. Chem.* **2006**, *16*, 1121–1124.
(61) Gosar, P.; Choi, S. I. *Phys. Rev.* **1966**, *150*, 529–538.
(62) Troisi, A.; Orlandi, G. *J. Phys. Chem. A* **2006**, *110*, 4065–4070.
(63) Troisi, A.; Orlandi, G. *Phys. Rev. Lett.* **2006**, *96*, 086601.
(64) Martinelli, N. G.; Olivier, Y.; Athanasopoulos, S.; Ruiz-Delgado, M. C.; Pigg, K. R.; da Silva, D. A.; Sánchez-Carrera, R. S.; Venuti, E.; Della Valle, R. G.; Brédas, J. L.; Beljonne, D.; Cornil, J. *Chemphyschem* **2009**, *10*, 2265–2273.
(65) Ruiz-Delgado, M. C.; Pigg, K. R.; da Silva Filho, D. A.; Gruhn, N. E.; Sakamoto, Y.; Suzuki, T.; Osuna, R. M.; Casado, J.; Hernández, V.; Navarrete, J. T. L.; Martinelli, N. G.; Cornil, J.; Sánchez-Carrera, R. S.; Coropceanu, V.; Brédas, J.-L. *J. Am. Chem. Soc.* **2009**, *131*, 1502–1512.
(66) Troisi, A. *Adv. Mater.* **2007**, *19*, 2000–2004.
(67) Sleigh, J. P.; McMahon, D. P.; Troisi, A. *Appl. Phys. A* **2009**, *95*, 147–152.
(68) Hannewald, K.; Bobbert, P. A. *Appl. Phys. Lett.* **2004**, *85*, 1535–1537.
(69) Munn, R. W.; Silbey, R. *J. Chem. Phys.* **1985**, *83*, 1843–1853.
(70) Munn, R. W.; Silbey, R. *J. Chem. Phys.* **1985**, *83*, 1854–1864.
(71) Holstein, T. *Ann. Phys.* **1959**, *8*, 325–342.
(72) Holstein, T. *Ann. Phys.* **1959**, *8*, 343–389.
(73) Kwiatkowski, J. J.; Frost, J. M.; Kirkpatrick, J.; Nelson, J. *J. Phys. Chem. A* **2008**, *112*, 9113–9117.
(74) Wang, L. J.; Peng, Q.; Li, Q. K.; Shuai, Z. *J. Chem. Phys.* **2007**, *127*, 044506.

JP910102F